View metadata, citation and similar papers at core.ac.uk

brought to you by CORE

provided by NASA Technical Reports Server

NASA TN D-932

TECHNICAL NOTE

D-932

BOUNDARY-LAYER TRANSITION ON A GROUP OF BLUNT NOSE SHAPES AT A MACH NUMBER OF 2.20

By Mary W. Jackson and K. R. Czarnecki

Langley Research Center
Langley Field, Va.

NATIONAL AERONAUTICS AND SPACE ADMINISTRATION

WASHINGTON

July 1961

N

NATIONAL AERONAUTICS AND SPACE ADMINISTRATION

TECHNICAL NOTE D-932

BOUNDARY-LAYER TRANSITION ON A GROUP OF BLUNT NOSE SHAPES AT A MACH NUMBER OF 2.20

By Mary W. Jackson and K. R. Czarnecki

L
1
3
8
3

SUMMARY

An investigation has been made to study boundary-layer transition on six axisymmetrical blunt bodies of revolution. Model shapes were selected with respect to the degree of favorable pressure gradient over the model surface. Tests were conducted at a Mach number of 2.20 and over a range of free-stream Reynolds number per foot of about 1.4×10^6 to 6.5×10^6. The tests were made at an angle of attack of 0° with zero heat transfer.

For the hemisphere, the flow remained essentially laminar over the model surface length for the entire pressure range of the tests. For a strong favorable pressure gradient followed by any weak favorable, neutral, or adverse gradient, the tendency was for transition to occur at or immediately behind the shoulder. A single strip of three-dimensional roughness in the region of strong favorable pressure gradient did not fix transition on the models at the roughness location except at the maximum test pressures, whereas a second roughness strip added in a region of neutral or adverse pressure gradient did fix transition. Experimental pressure coefficients agreed closely with modified Newtonian theory except in the shoulder region.

INTRODUCTION

Boundary-layer transition has an important influence on local surface temperatures and heat-transfer rates. In order to approach optimum design of missile noses, reliable knowledge of the factors controlling transition must be known. Several boundary-layer transition investigations have been made on various shapes, but there is still a need for data from a group of systematically selected shapes tested in a single facility in which the turbulence level and local flow irregularities are apparently small.

The present investigation was undertaken to study boundary-layer transition on six blunt axisymmetrical bodies of revolution. The model shapes were selected with regard to the degree of favorable pressure gradient over the model surface and varied from a hemispherical shape to a flat-faced cylindrical shape.

All tests were conducted at a free-stream Mach number of 2.20 over a range of free-stream Reynolds number per foot of about 1.4×10^6 to 6.5×10^6. All data were taken with the models at zero angle of attack and under essentially zero heat-transfer conditions.

L
1
3
8
3

SYMBOLS

C_p	pressure coefficient
M_l	local Mach number at outer edge of boundary layer
p_l	local static pressure on model surface, lb/sq ft
p_t'	stagnation-point pressure behind normal shock, lb/sq ft
N_{Pr}	Prandtl number
r	radius, in.
R	free-stream Reynolds number per foot
R_θ	Reynolds number based on momentum thickness and local conditions at outer edge of boundary layer
s	surface distance measured from stagnation point, in.
T_t	free-stream stagnation temperature, $^\circ R$
T_r	recovery temperature, $^\circ R$
η_r	recovery factor
γ	ratio of specific heats

APPARATUS AND METHODS

Wind Tunnel

The investigation was conducted in the Langley 4- by 4-foot supersonic pressure tunnel, which is a rectangular, closed-throat, single-return tunnel with provisions for the control of pressure, temperature, and humidity of the enclosed air. The investigation was conducted at a free-stream Mach number of 2.20. During the tests, the dewpoint was kept below -20° F at atmospheric pressure; therefore, the effects of water condensation in the supersonic nozzle were negligible.

L
1
3
8
3

Models

Six models with varying nose bluntness and pressure gradients were used in this investigation. Sketches of these models are shown in figure 1. The range of configurations extended from a hemispherical body with a completely favorable pressure gradient (model A) through a range of nose shapes with varying amounts of less favorable pressure gradients and adverse pressure gradient. The skin of each model was of 0.090-inch-thick 347 stainless steel. In order that a common mount might be used for all models, all base diameters were 12.00 inches. All models were sting mounted for the tests. Surface roughness of the smooth models was less than 5 microinches root mean square. Carborundum grit with a maximum measurement of 0.039 inch was arbitrarily used to fix transition on the model. This large-size grit protruded through the boundary layer but was chosen because past tests in this tunnel had indicated some problem in fixing transition at the roughness with smaller grain sizes on bodies with large favorable pressure gradients.

Instrumentation

Each model was instrumented with a row of no. 30 gage iron-constantan thermocouples which extended from the stagnation point along the upper generatrix of the body to near the model base. The thermocouples were spot-welded to the inner surface of the model and the temperature data were recorded on Brown potentiometer recorders. The voltage output of each thermocouple was recorded every 12 seconds. Temperatures were read from the temperature charts to the nearest 0.5° F. A row of pressure orifices (0.050-inch outside diameter, 0.040-inch inside diameter) were located 1/2 inch to $1\frac{1}{2}$ inches apart along a longitudinal line 90° from the thermocouple locations. Care was taken to locate more orifices in the model shoulder region, where a rapid change takes place in flow over the model, so as to obtain better defined

pressure distributions in that region. The pressure orifices were connected to mercury manometers which indicated surface pressure measurements. A list of the locations of the thermocouples and pressure orifices for each model is given in table I.

A twin-mirror schlieren system was employed to aid in determining the type of boundary-layer flow over the models.

Tests

All tests were conducted with the models at an angle of attack of 0° and at a free-stream Mach number of 2.20. Tunnel stagnation pressures varied from approximately 800 to 4,300 pounds per square foot, which corresponds to a range of free-stream Reynolds number per foot of 1.4×10^6 to 6.5×10^6. The tunnel stagnation temperatures varied from about 535° R to 580° R.

The test procedure consisted in starting at low tunnel stagnation pressures and advancing to the higher pressures. Whenever data were to be recorded, the tunnel was brought to and held at the desired tunnel condition until the temperatures reached equilibrium. All equilibrium temperatures were recorded for a period of at least 60 seconds. Simultaneously, photographs were taken of the multiple-tube mercury manometer to which the pressure tubes were connected and schlieren photographs were made of the flow over the models.

Data Reduction

In order to obtain reasonably accurate predicted temperature distributions, experimental pressure distributions were desirable as a basis for theoretical calculations. The pressure distributions were reduced in the usual manner.

Calculations of T_r/T_t were made from the relationship

$$\frac{T_r}{T_t} = \left(1 + \frac{\gamma - 1}{2} \eta_r M_l^2\right)\left(\frac{p_l}{p_t'}\right)^{\frac{\gamma-1}{\gamma}}$$

where T_r is the recovery temperature, $\eta_r = \sqrt{N_{Pr}}$ for the laminar boundary layer, $\eta_r = \sqrt[3]{N_{Pr}}$ for the turbulent boundary layer, and the Prandtl number is constant at 0.73. The value of N_{Pr} was selected to give the best overall fit to the experimental data.

Experimental temperature distributions over the models were read directly from Brown potentiometer recorders. At each longitudinal station, five recorded skin temperatures were averaged and the average value was treated as a single temperature reading. Temperature readings were then reduced to a ratio by dividing the local wall temperature by the measured model stagnation-point temperature. Because of the small temperature difference on the models and the thin skin, no correction was made for longitudinal heat conduction. Because of the relatively small skin thickness and assumed zero heat-transfer condition, no correction was applied for installation of the thermocouples on the inner surface of the models.

L
1
3
8
3

RESULTS AND DISCUSSION

Pressure Distribution

Experimental pressure-coefficient distributions over the bodies of the six configurations were obtained to provide a reasonably accurate basis for computing the recovery temperature ratios T_r/T_t for the laminar and turbulent boundary layers. Comparisons of these calculated ratios with the experimental data provided a means by which transition could be detected. The pressure data are presented in figures 2 to 7. As a matter of interest, the experimental pressures are compared with theoretical curves from modified Newtonian theory, in which $C_p = C_{p_t}' \sin^2\delta$, where C_{p_t}' is the pressure coefficient at the model stagnation point and δ is the angle between the surface and the stream direction.

Since fixing transition on the models did not have a significant effect on the pressure distributions, smooth-model data only are presented in figures 2 to 7. The data, in general, show no effect of Reynolds number on pressure distribution.

The hemispherically shaped model A had a very strong favorable pressure gradient over its entire length. As expected, the experimental pressure distributions compared favorably with theory for model A. Previous studies have shown that modified Newtonian theory gives reasonably good agreement with experiment on hemispheres even at a Mach number of 2.20. (For example, see ref. 1.)

Models B, C, D, and E form a family of blunt noses. The shapes begin as a hemisphere-cone and change progressively to blunter and blunter faces, maintaining rounded shoulders, but decreasing the cone angle of the afterbody at the base until a flat-faced, round-shouldered,

cylindrical shape, model E, is reached. (See fig. 1.) The pressure distributions for the group (figs. 3 to 6) show a fairly similar trend: weaker gradients on the face as the nose shape becomes blunter, strong favorable gradients at the shoulders, and weak favorable or adverse gradients on the sides of the models. The data show that increasing the amount of face blunting resulted in an increase in the surface distance from the stagnation point to the expansion of flow ahead of the shoulder. The smaller the cone angle of the model afterbody, the greater the distance required for recompression after overexpansion of the flow at the shoulder. In general, the experimental data were in agreement with the theoretical calculations over the front face of the models. In the shoulder region, however, the experimental pressure coefficients were more negative than predicted. Agreement of experimental data with theory rearward of this shoulder region became poorer with decreases in the cone angle of the model afterbody.

L 1 3 8 3

Model F, the flat-faced cylindrical model, exhibited expansion of flow very far ahead of the shoulder, a very steep pressure rise at the shoulder, and negative pressures beyond the shoulder. (See fig. 7.) The indication is that the flow was separated in the region beyond the shoulder. Schlieren photographs confirm the fact. Although separation occurred for the sharp-shouldered model F, it did not occur for the round-shouldered model E (fig. 6). (Model E differs from model F only in the shape of the shoulder.)

Recovery-Temperature Ratios

The results of the recovery-temperature investigation are presented in figures 8 to 13. Experimental recovery-temperature ratios are compared with theoretical ratios over a range of free-stream Reynolds number per foot of 1.4×10^6 to 6.5×10^6 for natural- and fixed-transition models. An attempt was made to fix transition on the models so as to establish recovery-temperature ratios for a known turbulent boundary layer and to aid in the interpretation of the results of the smooth-model investigation.

For the smooth hemispherical model A, the experimental temperature distributions (fig. 8) showed good agreement with laminar theory throughout the pressure range over the model surface. The rise in temperature at the last thermocouple location is ascribed to heat transfer to the model surface from the base of the model. Examination of schlieren photographs indicates that the flow was laminar at this location. Values of R_θ for the maximum free-stream Reynolds number per foot of 6.5×10^6 were computed by using the basic approach of Cohen and Reshotko (ref. 2) as applied in reference 3. At 90° on the hemispherical nose, which is

equivalent to about $s = 9$ inches, R_θ was computed to be 700. This value of R_θ is less than the range of values, 900 to 1,000, found for the hemisphere-cone investigation of reference 3. Thus it appears that either a somewhat larger model or a somewhat higher tunnel pressure is necessary to cause transition on the surface of the hemispherical model.

For the fixed-transition model A, despite the fact that the roughness used was large enough to protrude through the boundary layer, the flow over the entire model was laminar for free-stream Reynolds numbers per foot smaller than 2.7×10^6. At a free-stream Reynolds number per foot of 3.4×10^6, it appears that the boundary layer began to change from laminar to transitional a short distance downstream of the roughness. The flow never became fully turbulent, however, even toward the rear of the model. Increasing the Reynolds number per foot caused the temperature ratios at all points on the model to the rear of the roughness to approach the theoretical turbulent values, but apparently the boundary layer still was transitional in nature even at the highest test Reynolds number per foot. The indication of a fully turbulent flow at $s = 9$ inches when $R = 6.5 \times 10^6$ is discounted because, as in the case of the smooth model, the temperature at this station is believed to be affected by the heat flow from the model base.

The recovery temperatures for the hemisphere-cone model B are presented in figure 9. Experimental data for the smooth body were in good agreement with the theoretical laminar curve for all free-stream Reynolds numbers greater than 1.4×10^6. There is, however, a tendency for the temperatures over the face of the model to be somewhat lower than the theoretical temperatures for corresponding positions, while the temperatures over the rearward part of the model tend to be higher than the theoretical temperatures. It should be noted that because of the lower velocities on the face of the model, the average temperature through the boundary layer is higher than the temperature for the boundary layer near the rear of the model. Reference 4 indicates a higher Prandtl number for a higher average temperature. Calculations show that if the theoretical temperature-distribution curves calculated for a constant Prandtl number are corrected for a variable Prandtl number based on the average temperature through the boundary layer as it varies over the model, then the agreement between theory and experiment becomes equally good at all stations on the model. At a free-stream Reynolds number per foot of 1.4×10^6, the experimental data were lower than the theoretical laminar curve. At very low pressures it takes a long time to bring the model to equilibrium conditions, and at a free-stream Reynolds number per foot of 1.4×10^6 the model may not have been at equilibrium. Calculation of R_θ for the maximum free-stream Reynolds number per foot

(6.5×10^6) at the rearmost thermocouple station (s = 13 inches) yields a value of 560. This is below the value of transitional R_θ (range of 900 to 1,000) for a similar hemisphere cone reported in reference 3; thus laminar flow should be expected.

For the fixed-transition model, a strip of 0.025-inch to 0.028-inch carborundum grit in the region of favorable pressure gradient (the model face) was sufficient to cause the flow to be transitional for the lower pressures and fully turbulent for the higher pressures just downstream of the roughness location. The flow did not become fully turbulent for the lower pressures until a second roughness strip was added in the region of the adverse pressure gradient. The data shown in figure 9 are for model B with double transition strips.

L 1383

The results for model C are presented in figure 10. Smooth-model data over the test pressure range show a similar trend to the smooth-model data of model B except at maximum test pressure. At the maximum test free-stream Reynolds number per foot, the boundary-layer flow changed from laminar to transitional just behind the model shoulder and developed into a fully turbulent boundary layer near the rear of the model. Although this model has a neutral pressure gradient followed by a weak adverse pressure gradient behind the shoulder as compared with the weak adverse gradient of model B at a corresponding location, transition started earlier than on model B. The reasons for this phenomenon are not known. Schlieren photographs of the flow at this test condition could not be interpreted.

Boundary-layer flow for the fixed-transition model (0.039-inch granular roughness) remained laminar up to a location just downstream of the first roughness strip over the test pressure range. For the higher pressures the flow changed to fully turbulent a short distance from the roughness location. As with model B, it was not until after a second roughness strip was added in the region of neutral to weak adverse pressure gradient that the boundary-layer flow over the entire test range became fully turbulent.

Data for the smooth model D are presented in figure 11. Even for the maximum test free-stream pressure the flow did not become transitional until possibly the last 2 or 3 inches of the model, and even then the flow never became fully turbulent.

In general, results for the fixed-transition model (0.039-inch granular roughness) follow the results for models B and C in that a single strip of roughness in the region of favorable pressure gradient was not sufficient to fix transition, and transition was not fixed until a second roughness strip was added.

In figure 12, the change from a laminar to a transitional boundary layer on the smooth-body model E is shown to occur in the region just behind the shoulder. This model, which probably had the strongest adverse pressure gradient just behind the shoulder of all the models, appears to have transitional flow at the very lowest test Reynolds number per foot. Increasing the Reynolds number per foot caused the flow to approach the fully turbulent level more quickly.

Data for the fixed-transition model (0.039-inch granular roughness) followed the same trends as the data for the other round-shouldered fixed-transition models.

The results for model F, the flat-faced cylindrical model, are presented in figure 13. The flow is separated behind the shoulder of model F and the theoretical recovery temperatures for unseparated flow behind the shoulder cannot be used in the determination of transition.

Comparison of results for the fixed-transition model and the smooth model indicates that at 9 inches the experimental recovery temperature for the maximum test pressure appears to approach the theoretical turbulent curve. Schlieren photographs indicate that the reattachment point is in the vicinity of 9 inches in this case.

CONCLUDING REMARKS

Six shapes ranging from a hemisphere to a flat-faced cylinder were investigated over a range of free-stream Reynolds number per foot from 1.4×10^6 to 6.5×10^6. For the hemisphere, the flow remained essentially laminar over the model surface length for the entire pressure range of the tests. For a strong favorable pressure gradient followed by any weak favorable, neutral, or adverse gradient, the results show a tendency for transition to occur at or immediately behind the shoulder.

A single transition strip in the region of or ahead of a strong favorable pressure gradient was not effective in fixing transition on the models except at the maximum test pressures, whereas a second strip added in a region of neutral or adverse pressure gradient did fix transition.

Experimental pressure coefficients agree favorably with modified Newtonian theory except in the shoulder region and rearward of the

shoulder. Rearward of the shoulder, the agreement became poorer as the model afterbody cone angle decreased.

Langley Research Center,
National Aeronautics and Space Administration,
Langley Field, Va., May 25, 1961.

REFERENCES

1. Truitt, Robert Wesley: Hypersonic Aerodynamics. The Ronald Press Co., c.1959.

2. Cohen, Clarence B., and Reshotko, Eli: The Compressible Laminar Boundary Layer With Heat Transfer and Arbitrary Pressure Gradient. NACA Rep. 1294, 1956. (Supersedes NACA TN 3326.)

3. Czarnecki, K. R., and Jackson, Mary W.: Effects of Cone Angle, Mach Number, and Nose Blunting on Transition at Supersonic Speeds. NASA TN D-634, 1961.

4. Cohen, Nathaniel B.: Correlation Formulas and Tables of Density and Some Transport Properties of Equilibrium Dissociating Air For Use in Solutions of the Boundary-Layer Equations. NASA TN D-194, 1960.

L
1
3
8
3

TABLE I.- THERMOCOUPLE AND PRESSURE ORIFICE LOCATIONS

Thermocouple location		Pressure-orifice location	
Station	s, in.	Station	s, in.
Model A			
1	0	1	0
2	1.0	2	1.0
3	2.0	3	2.0
4	3.0	4	3.0
5	4.0	5	4.0
6	5.0	6	5.0
7	6.0	7	6.0
8	7.0	8	7.0
9	8.0	9	8.0
10	9.0	10	9.0
Model B			
1	0	1	0
2	1.0	2	1.0
3	3.0	3	2.0
4	4.0	4	3.0
5	5.0	5	3.5
6	7.0	6	4.0
7	8.0	7	4.5
8	9.0	8	5.0
9	10.0	9	5.5
10	11.0	10	6.0
11	12.0	11	6.5
12	13.0	12	7.0
		13	8.0
		14	9.0
		15	10.5
		16	12.0
		17	13.5
Model C			
1	0	1	0
2	1.0	2	1.0
3	2.0	3	2.0
4	3.0	4	3.0
5	4.0	5	3.5
6	5.0	6	4.0
7	6.0	7	4.5
8	7.0	8	5.0
9	9.0	9	5.5
10	10.0	10	6.0
11	11.0	11	6.5
12	12.0	12	7.0
		13	8.0
		14	9.0
		15	10.0
		16	11.0
		17	12.0

Thermocouple location		Pressure-orifice location	
Station	s, in.	Station	s, in.
Model D			
1	0	1	0
2	2.0	2	1.0
3	3.0	3	2.0
4	4.0	4	3.0
5	5.0	5	3.5
6	6.0	6	4.0
7	7.0	7	4.5
8	8.0	8	5.0
9	9.0	9	5.5
10	10.0	10	6.0
		11	6.5
		12	7.0
		13	8.0
		14	9.0
		15	10.0
Model E			
1	0	1	0
2	2.0	2	1.0
3	3.0	3	2.0
4	4.0	4	3.0
5	5.0	5	4.0
6	6.0	6	5.0
7	7.0	7	5.5
8	8.0	8	6.0
9	9.0	9	6.5
10	10.0	10	7.0
11	11.0	11	7.5
		12	8.0
		13	8.5
		14	9.0
		15	10.0
		16	11.0
Model F			
1	0	1	0
2	1.0	2	1.0
3	2.0	3	2.0
4	3.0	4	3.0
5	4.0	5	4.0
6	5.0	6	5.0
7	6.0	7	6.0
8	7.0	8	6.5
9	8.0	9	7.0
10	9.0	10	7.5
		11	8.0
		12	8.5
		13	9.0
		14	10.0
		15	11.0

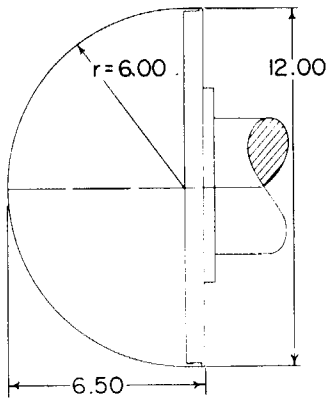

Model A

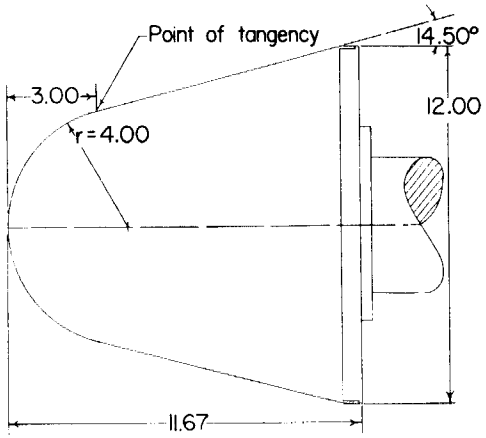

Model B

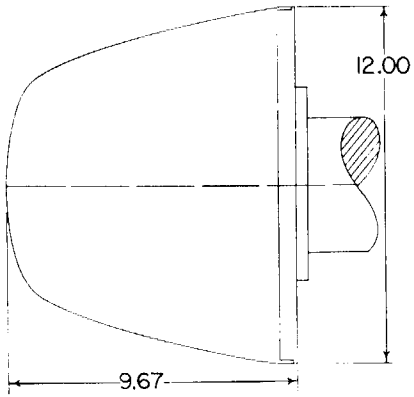

Model C

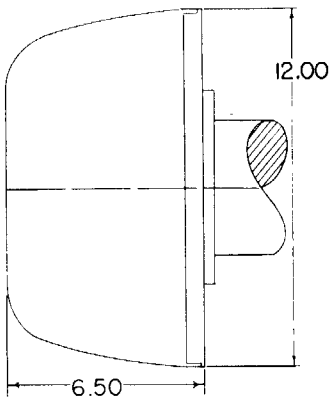

Model D

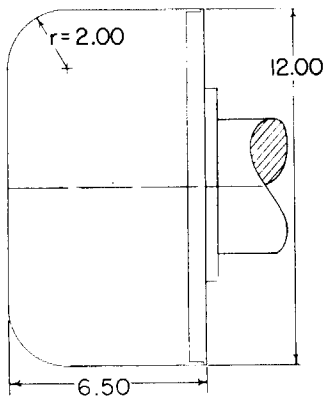

Model E

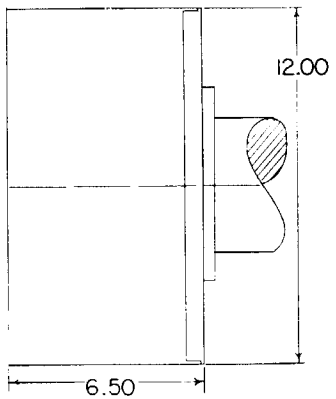

Model F

Figure 1.- Sketches of models. All dimensions are in inches unless otherwise indicated.

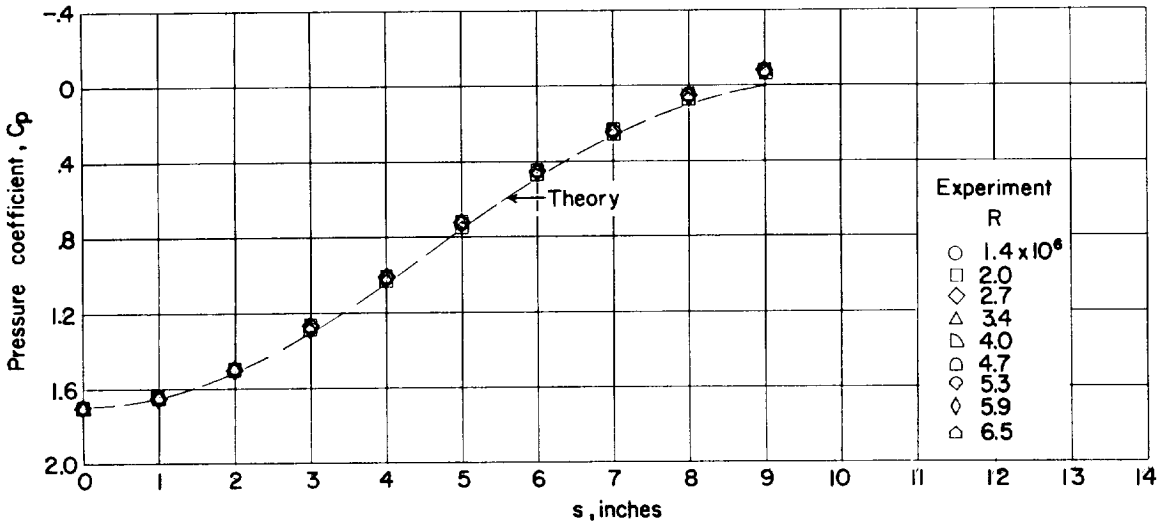

Figure 2.- Comparison of experimental pressure coefficients with calculated theoretical pressure coefficients for model A.

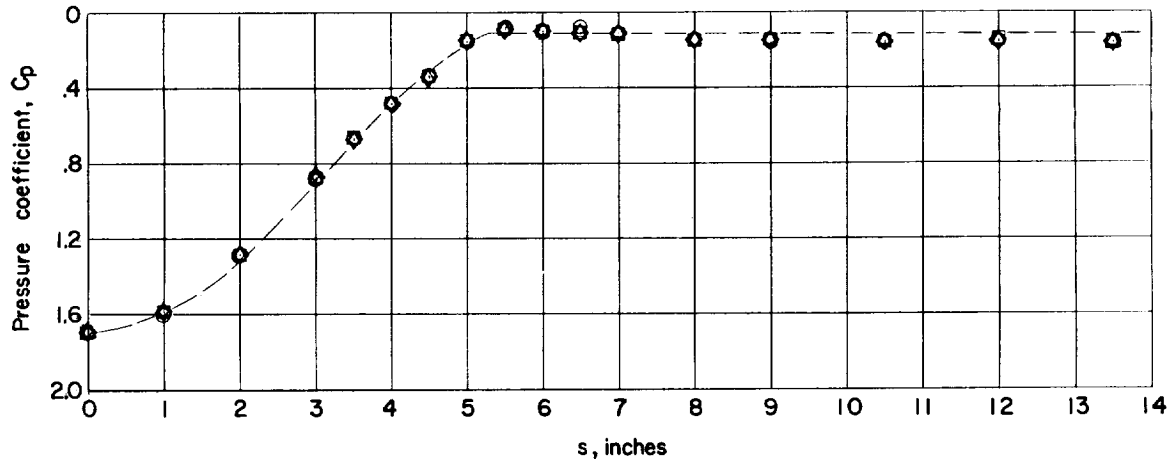

Figure 3.- Comparison of experimental pressure coefficients with calculated theoretical pressure coefficients for model B.

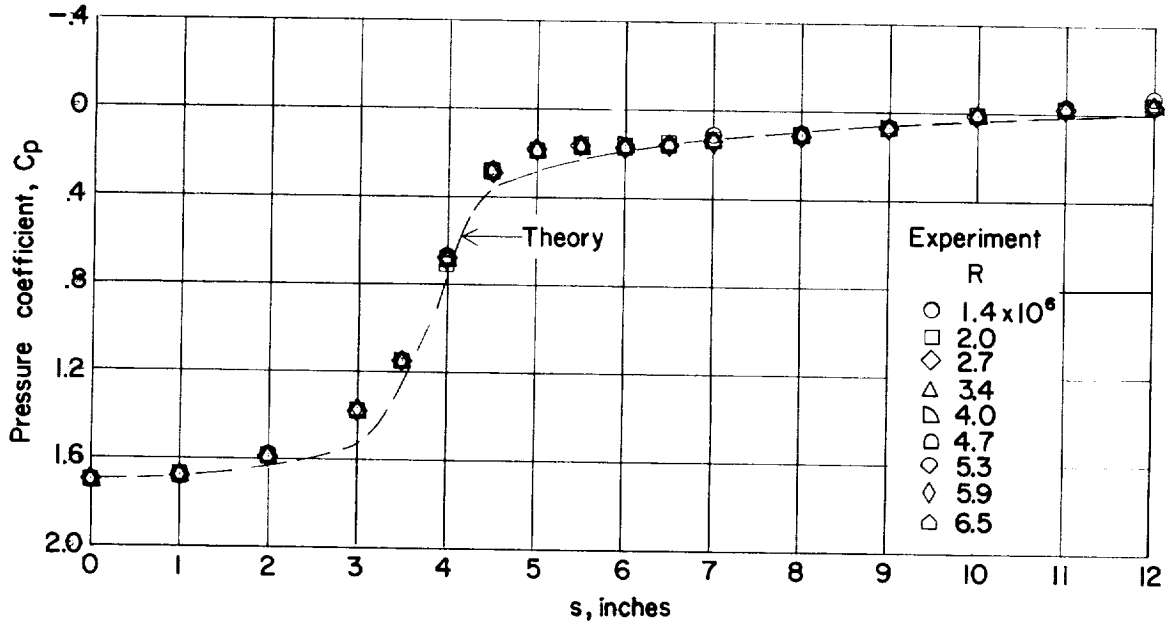

Figure 4.- Comparison of experimental pressure coefficients with calculated theoretical pressure coefficients for model C.

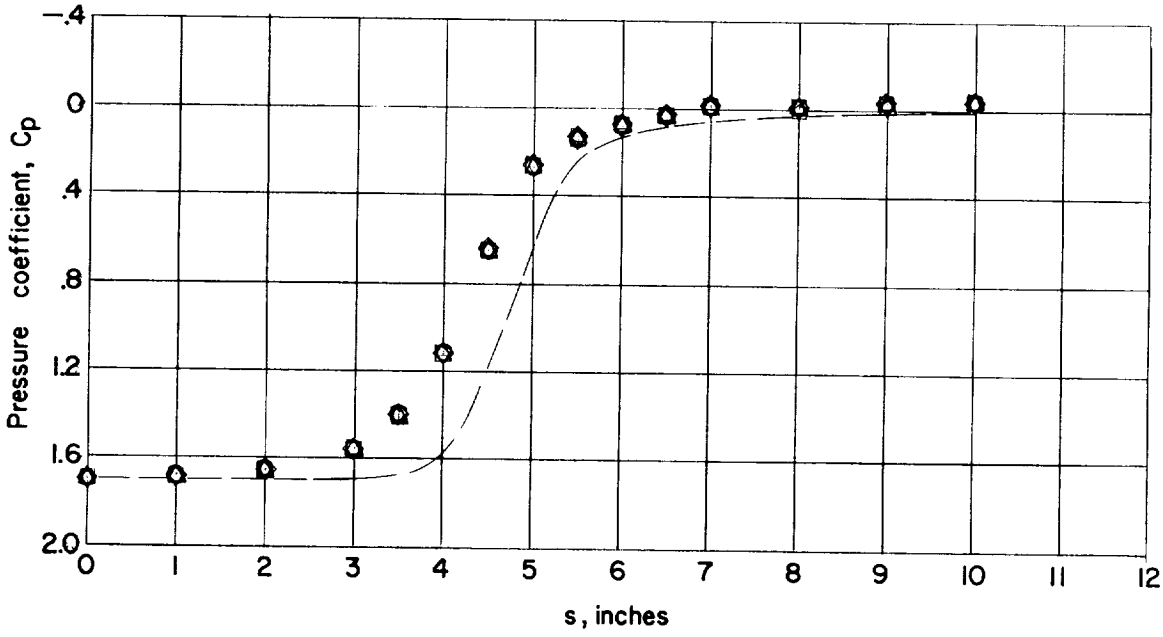

Figure 5.- Comparison of experimental pressure coefficients with calculated theoretical pressure coefficients for model D.

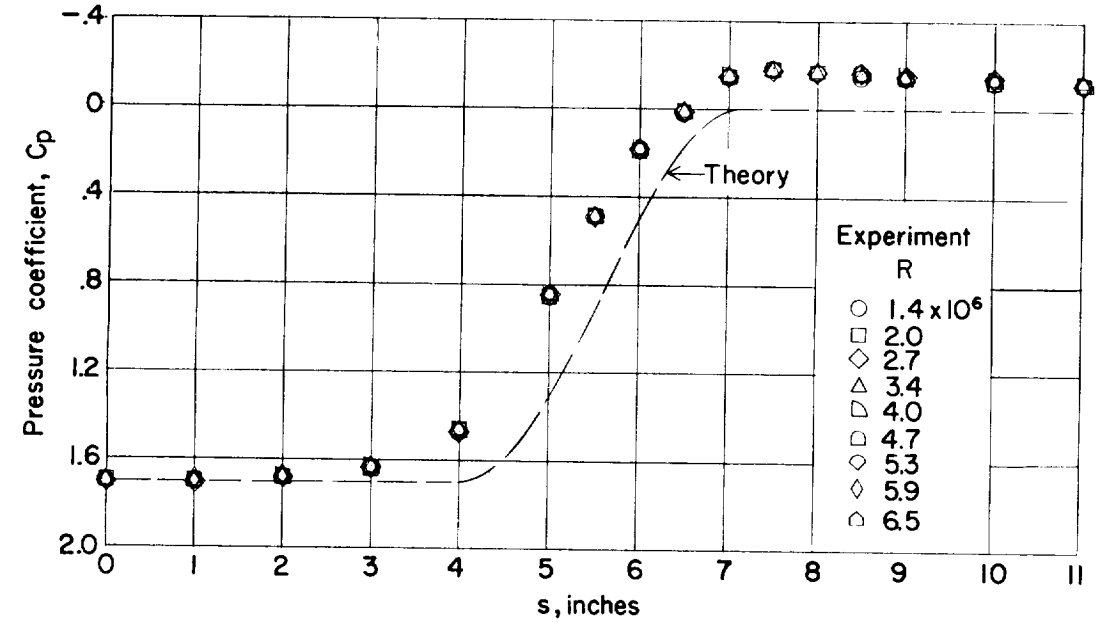

Figure 6.- Comparison of experimental pressure coefficients with calculated theoretical pressure coefficients for model E.

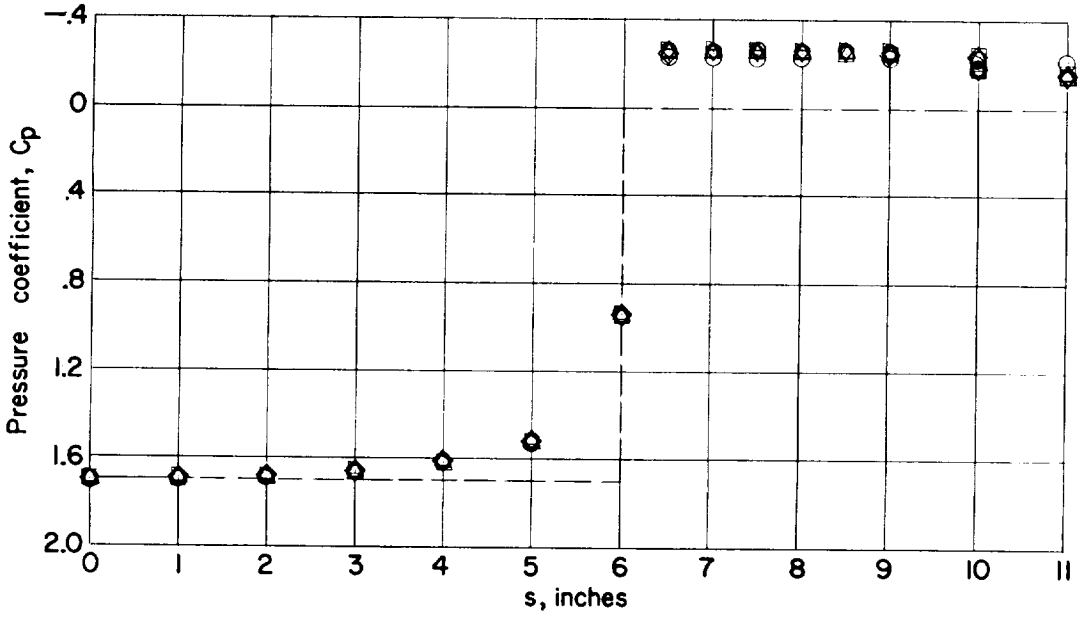

Figure 7.- Comparison of experimental pressure coefficients with calculated theoretical pressure coefficients for model F.

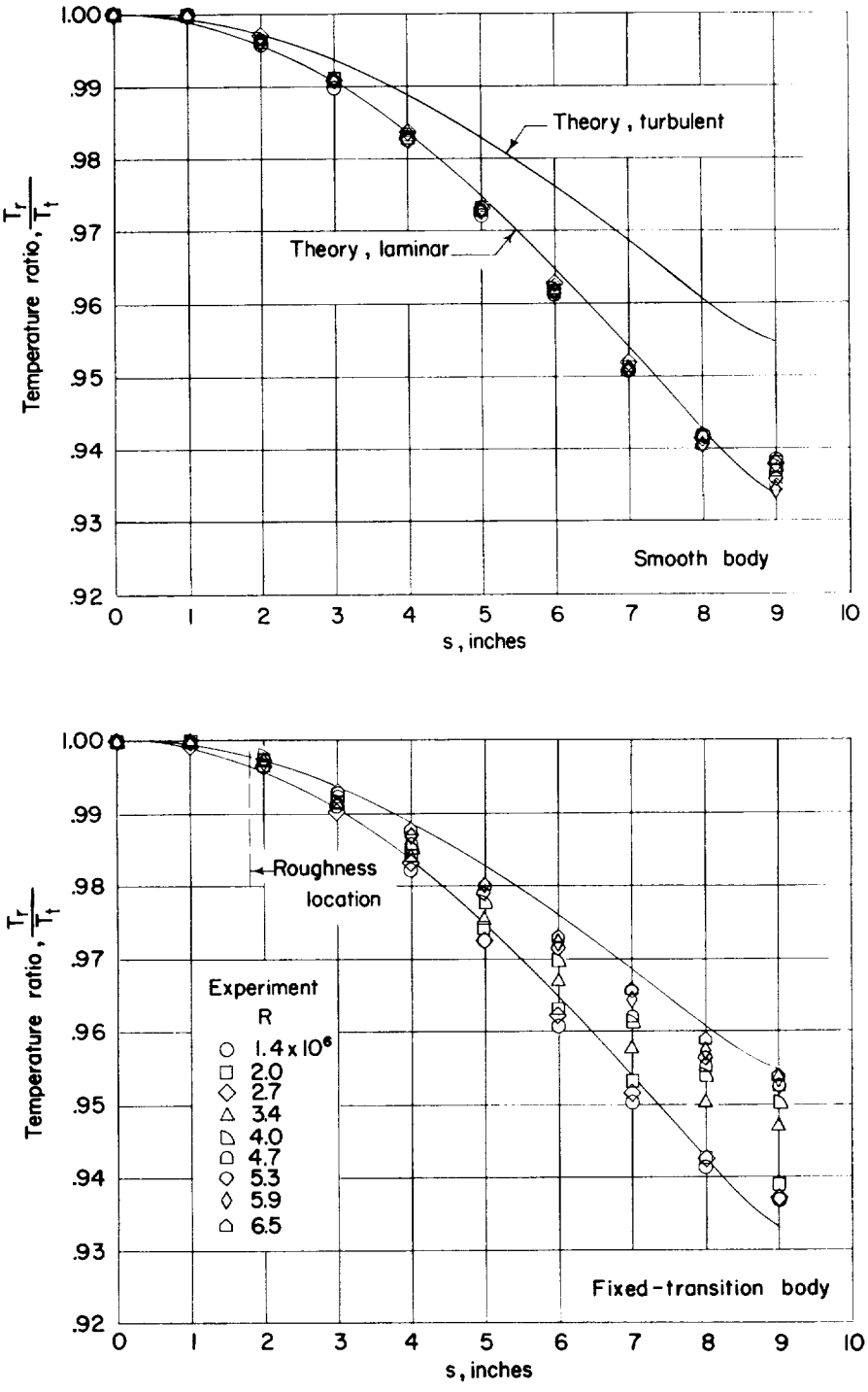

Figure 8.- Comparison of experimental recovery-temperature ratios with calculated recovery-temperature ratios for model A.

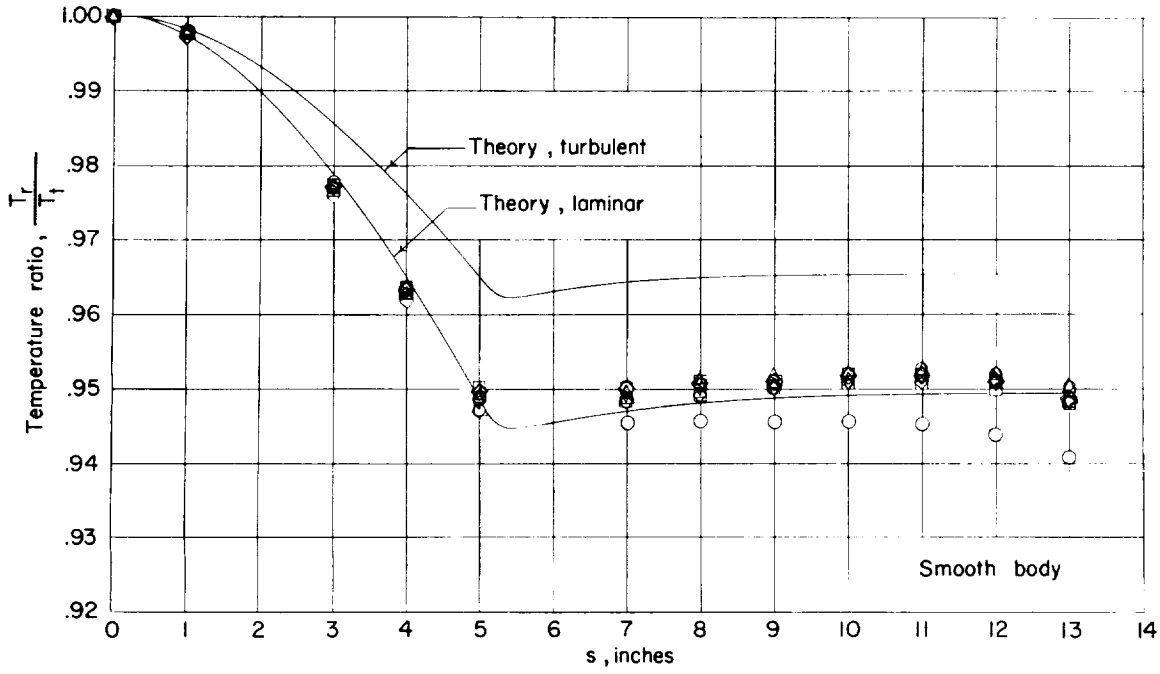

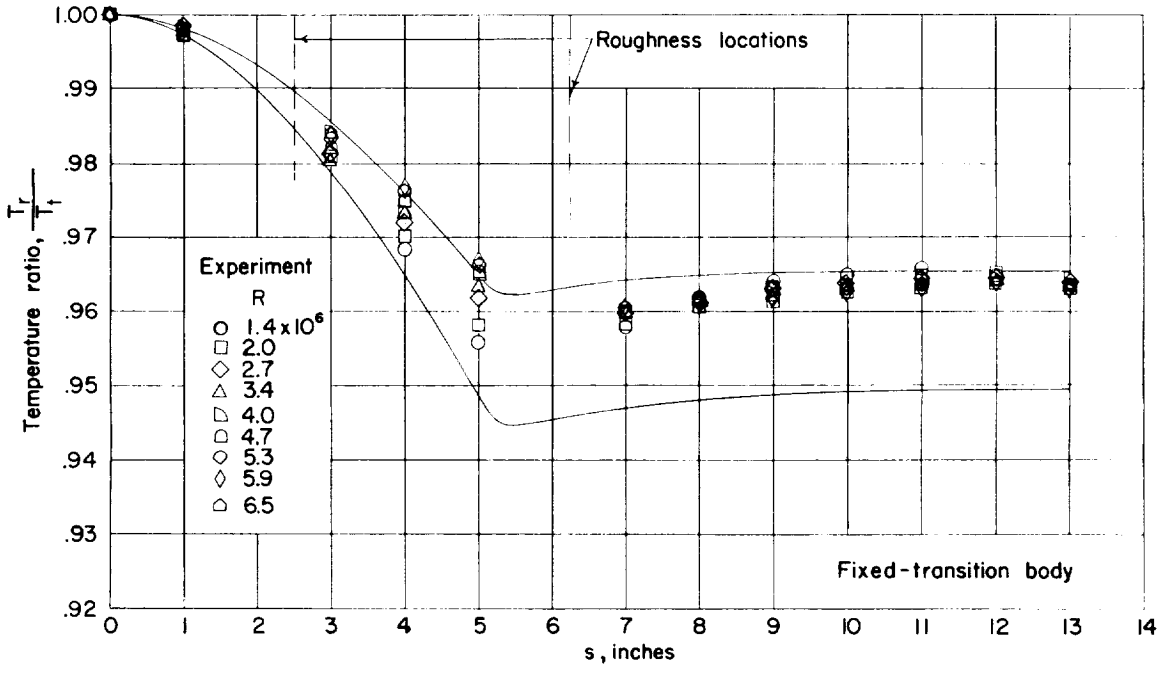

Figure 9.- Comparison of experimental recovery-temperature ratios with calculated recovery-temperature ratios for model B.

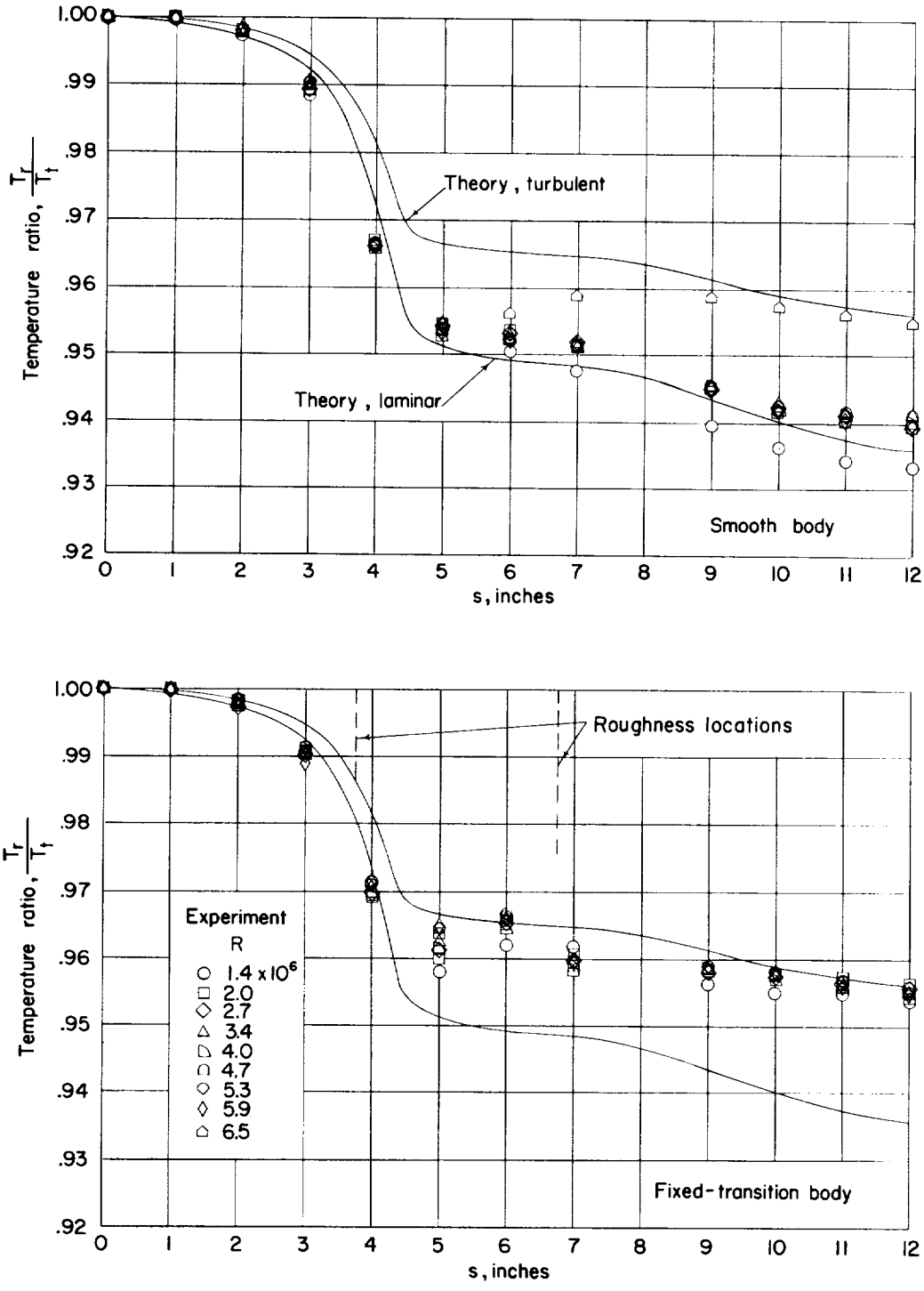

Figure 10.- Comparison of experimental recovery-temperature ratios with calculated recovery-temperature ratios for model C.

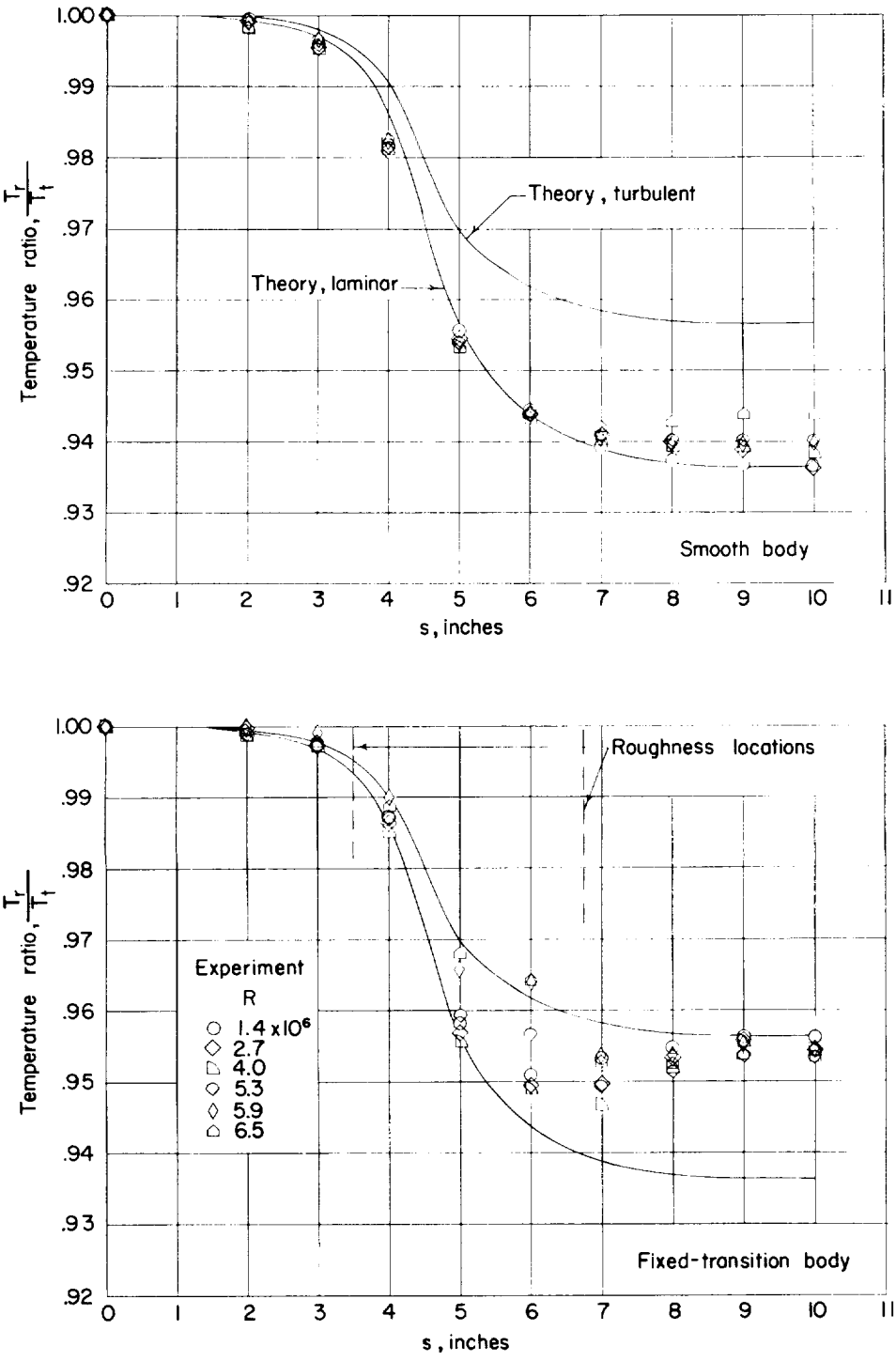

Figure 11.- Comparison of experimental recovery-temperature ratios with calculated recovery-temperature ratios for model D.

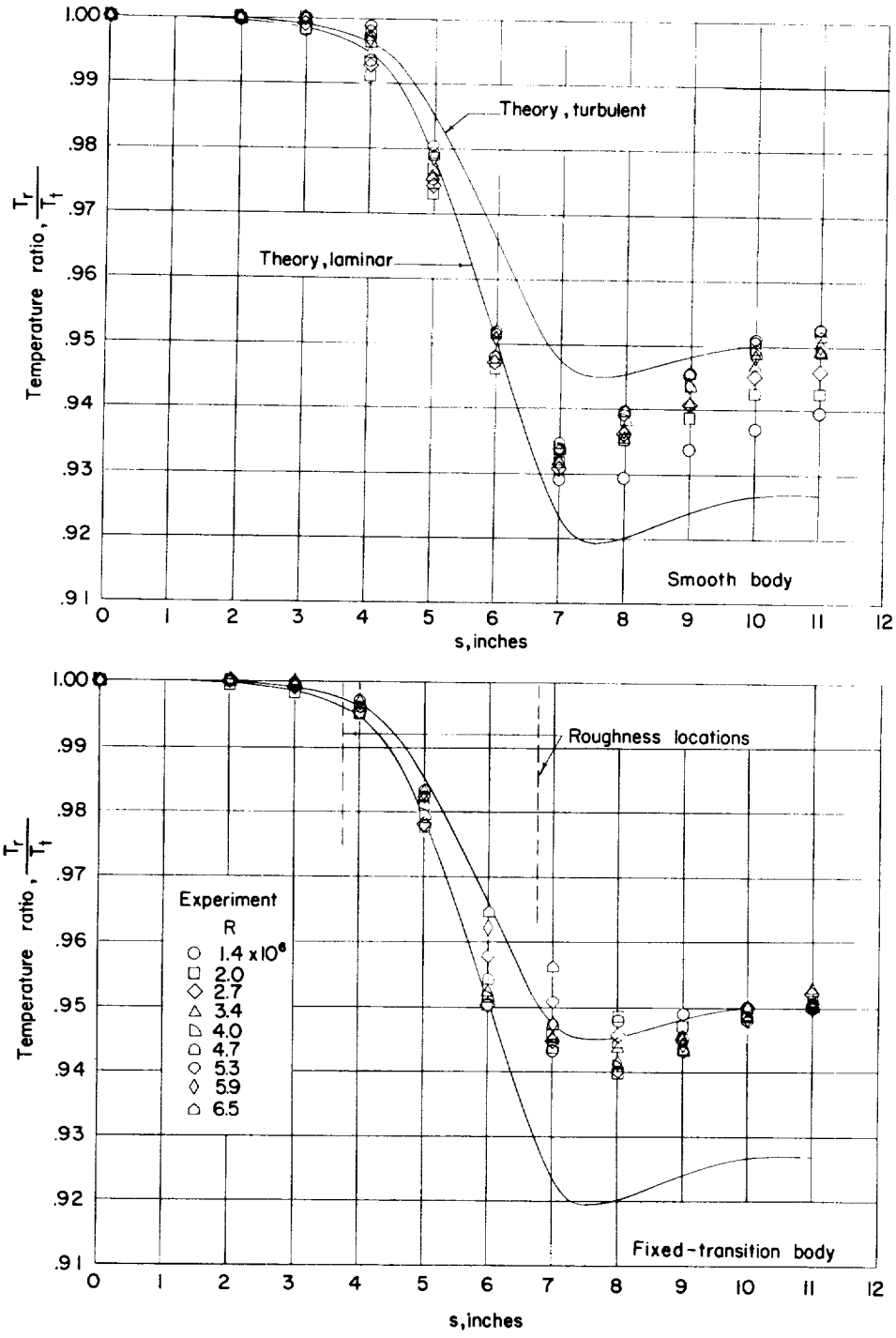

Figure 12.- Comparison of experimental recovery-temperature ratios with calculated recovery-temperature ratios for model E.

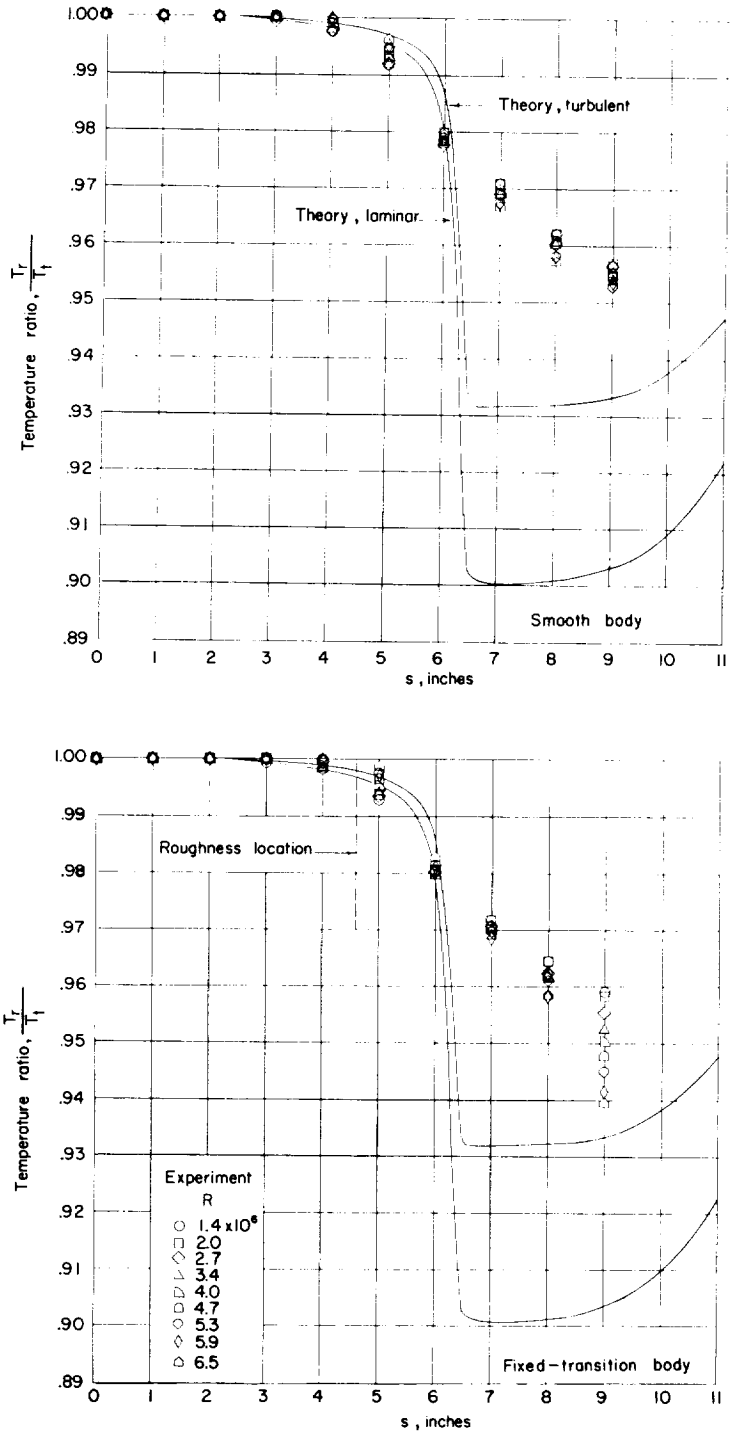

Figure 13.- Comparison of experimental recovery-temperature ratios with calculated recovery-temperature ratios for model F.

NASA TN D-932
National Aeronautics and Space Administration.
BOUNDARY-LAYER TRANSITION ON A GROUP OF BLUNT NOSE SHAPES AT A MACH NUMBER OF 2.20. Mary W. Jackson and K. R. Czarnecki. July 1961. 21p. OTS price, $0.75.
(NASA TECHNICAL NOTE D-932)

Six shapes ranging from a hemisphere to a flat-faced cylinder were investigated over a range of free-stream Reynolds number per foot from 1.4×10^6 to 6.5×10^6. For the hemisphere, the flow remained essentially laminar over the model surface length for the entire pressure range of the tests. For a strong favorable pressure gradient followed by any weak favorable, neutral, or adverse gradient, the results show a tendency for transition to occur at or immediately behind the shoulder. It was necessary to place a transition strip in a region of neutral or adverse pressure gradient to fix transition on the model.

Copies obtainable from NASA, Washington

I. Jackson, Mary W.
II. Czarnecki, Kazimierz Roman
III. NASA TN D-932

(Initial NASA distribution: 1, Aerodynamics, aircraft; 2, Aerodynamics, missiles and space vehicles; 20, Fluid mechanics.)

NASA

NASA TN D-932
National Aeronautics and Space Administration.
BOUNDARY-LAYER TRANSITION ON A GROUP OF BLUNT NOSE SHAPES AT A MACH NUMBER OF 2.20. Mary W. Jackson and K. R. Czarnecki. July 1961. 21p. OTS price, $0.75.
(NASA TECHNICAL NOTE D-932)

Six shapes ranging from a hemisphere to a flat-faced cylinder were investigated over a range of free-stream Reynolds number per foot from 1.4×10^6 to 6.5×10^6. For the hemisphere, the flow remained essentially laminar over the model surface length for the entire pressure range of the tests. For a strong favorable pressure gradient followed by any weak favorable, neutral, or adverse gradient, the results show a tendency for transition to occur at or immediately behind the shoulder. It was necessary to place a transition strip in a region of neutral or adverse pressure gradient to fix transition on the model.

Copies obtainable from NASA, Washington

I. Jackson, Mary W.
II. Czarnecki, Kazimierz Roman
III. NASA TN D-932

(Initial NASA distribution: 1, Aerodynamics, aircraft; 2, Aerodynamics, missiles and space vehicles; 20, Fluid mechanics.)

NASA

NASA TN D-932
National Aeronautics and Space Administration.
BOUNDARY-LAYER TRANSITION ON A GROUP OF BLUNT NOSE SHAPES AT A MACH NUMBER OF 2.20. Mary W. Jackson and K. R. Czarnecki. July 1961. 21p. OTS price, $0.75.
(NASA TECHNICAL NOTE D-932)

Six shapes ranging from a hemisphere to a flat-faced cylinder were investigated over a range of free-stream Reynolds number per foot from 1.4×10^6 to 6.5×10^6. For the hemisphere, the flow remained essentially laminar over the model surface length for the entire pressure range of the tests. For a strong favorable pressure gradient followed by any weak favorable, neutral, or adverse gradient, the results show a tendency for transition to occur at or immediately behind the shoulder. It was necessary to place a transition strip in a region of neutral or adverse pressure gradient to fix transition on the model.

Copies obtainable from NASA, Washington

I. Jackson, Mary W.
II. Czarnecki, Kazimierz Roman
III. NASA TN D-932

(Initial NASA distribution: 1, Aerodynamics, aircraft; 2, Aerodynamics, missiles and space vehicles; 20, Fluid mechanics.)

NASA

NASA TN D-932
National Aeronautics and Space Administration.
BOUNDARY-LAYER TRANSITION ON A GROUP OF BLUNT NOSE SHAPES AT A MACH NUMBER OF 2.20. Mary W. Jackson and K. R. Czarnecki. July 1961. 21p. OTS price, $0.75.
(NASA TECHNICAL NOTE D-932)

Six shapes ranging from a hemisphere to a flat-faced cylinder were investigated over a range of free-stream Reynolds number per foot from 1.4×10^6 to 6.5×10^6. For the hemisphere, the flow remained essentially laminar over the model surface length for the entire pressure range of the tests. For a strong favorable pressure gradient followed by any weak favorable, neutral, or adverse gradient, the results show a tendency for transition to occur at or immediately behind the shoulder. It was necessary to place a transition strip in a region of neutral or adverse pressure gradient to fix transition on the model.

Copies obtainable from NASA, Washington

I. Jackson, Mary W.
II. Czarnecki, Kazimierz Roman
III. NASA TN D-932

(Initial NASA distribution: 1, Aerodynamics, aircraft; 2, Aerodynamics, missiles and space vehicles; 20, Fluid mechanics.)

NASA